FLOW AND THERMAL CHARACTERISTICS OF NACA VORTEX GENERATOR WITH CURVED-DIVERGED WALLS

by

Houju PEI[a*], Yonglong CUI[b], Meinan LIU[c], and Kaijie YANG[d]

[a] Shanghai Aircraft Design and Research Institute, Shanghai, China
[b] Marine Design and Research Institute of China, Shanghai, China
[c] Jiangsu University of Science and Technology, Zhenjiang, China
[d] Nanjing University of Aeronautics and Astronautics, Nanjing, China

Original scientific paper
https://doi.org/10.2298/TSCI221231077P

Flow and heat transfer characteristics of NACA vortex generator with curved-divergent walls are numerically studied and the corresponding heat transfer enhancement mechanism is also analyzed by local streamlines, velocity vector diagram and velocity contour diagram. The variation of vortices at different positions along the flow direction is also illustrated. The impacts of the width, W, and height, H, on the heat transfer as well as pressure loss are investigated with Reynolds number ranging from 3602 to 9004. Additionally, both Nusselt number and Δp are considered when evaluating the comprehensive performance. The results show that as the width and height increase, the average Nusselt number and Δp increase as well. Compared with the channel without the NACA vortex generator, the average Nusselt number and Δp increased by about 7.3% and about 3.6%, respectively, by W = 30 mm; the average Nusselt number and Δp increased by about 7.6% and about 4.5%, respectively, by H = 10 mm. The variation of comprehensive performance shows an opposite trend. The η obtained the largest value of about 1.042 and 1.04 in the case of W = 10 mm and H = 4 mm, respectively. Additionally, the variation of the local Nusselt number is similar to that of the Y-vorticity.

Key words: *NACA vortex generator, pressure los, heat transfer, comprehensive performance*

Introduction

In the field of heat exchangers research, it is becoming increasingly important to improve heat transfer performance as much as possible with minimum pressure loss. As a kind of passive heat transfer enhancement device, the vortex generators (VG) have been widely used to reduce the air-side thermal resistance. The vortices will be generated as the fluid-flows through the VG, which will increase the turbulence of the fluid and destroy the thermal boundary-layer near the wall, thus enhancing the heat transfer ability [1]. Figure 1 shows several types of VG.

The VG are small aerodynamic devices that are commonly used to improve the performance of aircraft, wind turbines, and other structures that interact with fluid-flow. They are designed to manipulate the air-flow around these structures and achieve specific goals, such as increasing lift, reducing drag, or improving stability [2]. Since then,

* Corresponding author, e-mail: hj_pei@nuaa.edu.cn

researchers have conducted many experimental investigations and numerical simulations on heat transfer and pressure loss of winglet VG. The effects of arc-shaped and straight delta-winglet VG on the characteristics of finned tube heat exchangers are investigated by Su *et al*. [3]. As the Reynolds number changes from 500 to 5000, both VG can improve the heat transfer ability. As well, the straight delta-winglet has a slightly stronger enhancement effect than an arc-shaped one, but it has a higher pressure loss. For delta-winglet and rectangular-winglet configurations, Silvia *et al*. [4] analyzed the comprehensive characteristics of heat transfer and flow. When the angle of attack is 45°, both VG exhibit the best heat transfer performance, but the rectangular-winglet VG is more pronounced. Song *et al.* [5] claimed that the delta-winglet with a concave curved shape is helpful to improve heat transfer performance, while the delta-winglet with a convex curved shape has the reverse impact. The thermal characteristics of the wavy finned tube heat exchanger with a staggered concave curved VG are investigated by Hu *et al.* [6]. The VG can produce longitudinal vortices and improve heat transfer by 30.4%. In addition, the influence of the pair roll angle of the rectangular winglet on the distribution of local Nusselt number was also studied by Khanjian *et al.* [7]. Geometric optimization of VG still has great potential for improving heat transfer. The genetic algorithms are used to optimize the geometry of VG by Moreno *et al.* [8], and the positions and angles of the winglet-type VG are also optimized by RSM and DOM by Leandro *et al.* [9].

Although the winglet VG can increase the local Nusselt number, their pressure loss is large. This is not very desirable. Some researchers have studied the performance of cylindrical VG (such as cylinder, elliptic cylinder, oblique-cut cylinders, *etc.*). Esmaeilzadeh *et al.* [10] numerically deliberated that trapezoidal winglet pair (TWP) has a higher pressure loss and a worse overall performance compared to curved (TWP) (CTWP). According to their findings, CTWP outperforms TWP in terms of overall performance and pressure loss.

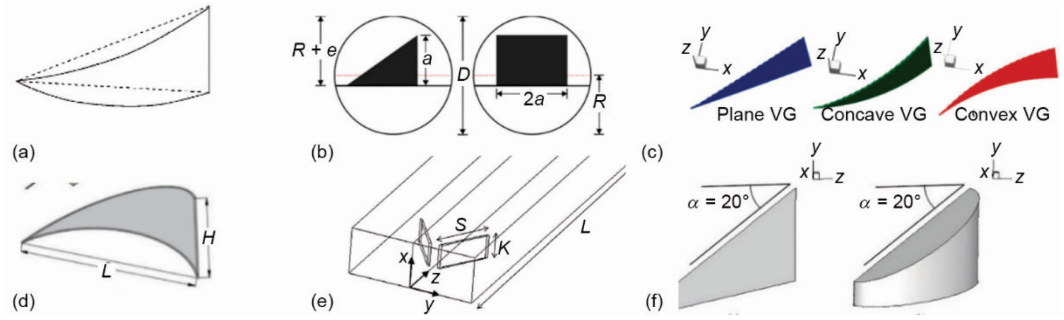

Figure 1. Geometry of common VG; (a) straight delta-winglet and arc-shaped VG [3], (b) delta-winglet and rectangular-winglet VG [4], (c) plane VG, concave VG, and convex VG [5], (d) staggered curved VG [6], (e) rectangular winglet [7], and (f) simple trapezoidal VG and curved trapezoidal VG [11]

In summary, there are many studies on heat transfer enhancement using VG, most of which are winglet or cylindrical type. However, according to our previous investigations [12], very little research has been published on the newly designed NACA vortex generator (NVG). The main idea of this study is to predict the flow and heat tansfer characteristics in the range of Reynolds number from 3602 to 9004 using the verified CFD scheme. The mechanism of heat transfer enhancement is analyzed by the velocity streamlines and vorticity distribution contours. The effects of width and height on its performance are also discussed.

Computational models

Figure 2 illustrates the computational models of the rectangular channel with the NVG. The test section is 1000 mm × 200 mm × 50 mm, fig. 2(a). In consideration of the complete turbulence in the test section and to avoid backflow, two extended sections are added. The NVG is placed in the center of the bottom surface. Utilized is a curved-divergent wall, fig. 2(b), and the co-ordinates of control points are shown in [13]. The NVG is characterized by height, H, fig. 2(c), length, L, and width, W. The parameters and values of the NVG for numerical simulations are shown in tab. 1. The initial parameters are H = 6 mm, W = 30 mm, and L = 100 mm.

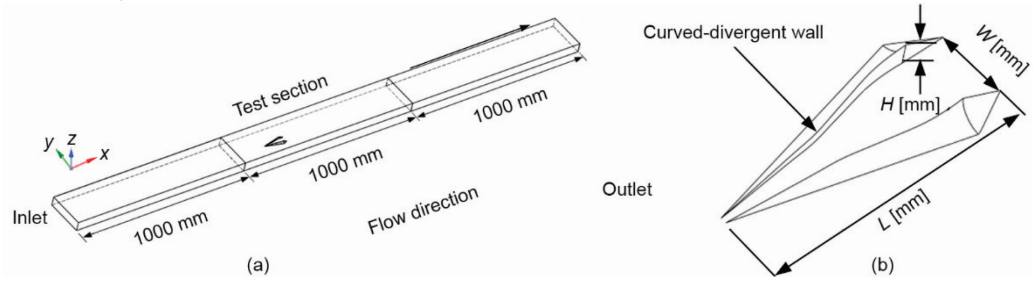

Figure 2. The schematic views of the rectangular channel with NVG: (a) computational domain and (b) the details of the *W*, *L*, and *H*

Table 1. Parameters and values of NVG

L [mm]	W [mm]	H [mm]
100	30	6
100	10, 20, 25, 30	6
100	30	4, 6, 8, 10

Numerical method

Governing equation

The air in the rectangular channel is regarded as incompressible fluid and in a completely turbulent state. Governing equations are written as follows [14]:

Continuity equation

$$\frac{\partial}{\partial x_i}(\rho u_i) = 0 \tag{1}$$

where u is the velocity and ρ – the density.

Momentum equation

$$\frac{\partial}{\partial x_j}(\rho u_i u_j) = -\frac{\partial p}{\partial x_i} + \frac{\partial}{\partial x_j}(\mu + \mu_t)\left(\frac{\partial u_i}{\partial x_j} + \frac{\partial u_j}{\partial x_i}\right) \tag{2}$$

where μ is the dynamic viscosity, p – the pressure, and μ_t – the turbulent viscosity.

Energy equation

$$\frac{\partial}{\partial x_i}(u_i T) = \frac{\partial}{\partial x_i}\left[\left(\frac{\mu}{\mathrm{Pr}} + \frac{\mu_t}{\mathrm{Pr}_t}\right)\frac{\partial T}{\partial x_i}\right] \tag{3}$$

where Pr – is the Prandtl number and T – the temperature.

The numerical simulation is carried out by the commercial software FLUENT. The second-order upwind scheme and the coupled algorithm are chosen. The residuals of the equations are controlled at 10^{-6}. The validated turbulence model of k-ε will be used [15].

Mesh

As shown in fig. 3(a), a polyhedral grid is used in the computational domain. To balance the calculation accuracy and computational efficiency, the grid near the NVG is as dense as possible, while the grid is relatively sparse in other areas. Considering that the turbulent viscosity of the fluid close to the wall is much smaller than the molecular viscosity, and the vortex structure near the NVG should be observed, the computational grids close to the wall are processed by the wall function. The prism grids are shown in fig. 3(b). The growth rate is 1.2, the number of prism layers is 10, the total boundary-layer thickness is $1 \cdot 10^{-3}$ m, and the number of cells are about 1000000.

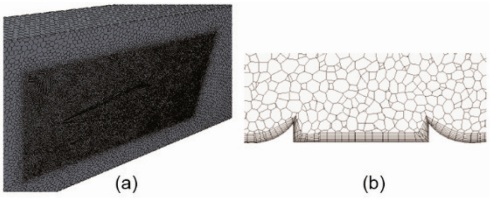

Figure 3. Grid system; (a) grids of the computational domain and (b) prism grids close to the NVG

Boundary conditions

The type of fluid is air, its working temperature is 318 K, density is 1.1105 kg/m^3, viscosity coefficient is $17.455 \cdot 10^{-6}$ m^2/s and Prandtl number is 0.6985. The inlet velocity is 0.431 m/s, 0.539 m/s, 0.647 m/s, 0.862 m/s, 0.970 m/s, 1.078 m/s. The corresponding Reynolds number is 3602, 4502, 5402, 6303, 8104, and 9004, respectively. The pressure of the outlet is 1 atmosphere. The temperature of the bottom wall is 343 K, and the other walls are set up as adiabatic wall. To eliminate the influence of heat conduction on the temperature field and flow field, the surface of the NVG is also set as an adiabatic wall. In addition, all the walls of the rectangular channel and the NVG surface are set as non-slip walls.

Dimensionless parameter

The formula for calculating pressure loss is [16]:

$$\Delta p = p_{\text{test-in}} - p_{\text{test-out}} \tag{4}$$

where subscript test-in and test-out represent the inlet and outlet of test, respectively, and p is the area-averaged total pressure.

Although the VG can enhance heat transfer, this process is often accompanied by a large pressure loss. Therefore, it is not comprehensive to just consider the heat transfer enhancement and ignore the pressure loss increase. A comprehensive criterion is used, whose definition [17] is:

$$\eta = \frac{\dfrac{h}{\Delta p}}{\dfrac{h_0}{\Delta p_0}} = \frac{\dfrac{h}{h_0}}{\dfrac{\Delta p}{\Delta p_0}} \tag{5}$$

where h is the heat transfer coefficient and subscript 0 represents the smooth rectangular channel (without NVG).

Grid refinement tests

To ensure that the results are independent of the grid number, grid refinement tests are carried out. The results are shown in tab. 2. The Nusselt number only changes by 1% as the grids number increase from 1000000 to 1200000. In order to keep a balance between the computational efficiency and accuracy, the grid system of 1000000 cells is chosen for the grid independence validation.

Table 2. Grid refinement tests (Re = 9,004)

Number of cells	Nusselt number	Number of cells	Nusselt number
800000	34.64	1000000	36.11
900000	35.52	1200000	36.54

Numerical method validation

The numerical results of the smooth rectangular channel were compared with those of Gnielikski's correlation [18] for Nusselt number to validate the numerical method:

$$\mathrm{Nu} = \frac{\frac{f}{8}(\mathrm{Re}-1000)\,\mathrm{Pr}}{1+12.7\left(\frac{f}{8}\right)^{\frac{1}{2}}\left(\mathrm{Pr}^{\frac{2}{3}}-1\right)}\left[1+\left(\frac{d}{l}\right)^{\frac{2}{3}}\right]c_t \tag{6}$$

$$c_t = \left(\frac{T}{T_{\mathrm{wall}}}\right)^{0.045} \tag{7}$$

where f is the Darcy drag factor, $f = (1.82\lg\mathrm{Re}-1.64)^{-2}$, d and l are the equivalent diameter and length of the flow channel, respectively, and c_t – the temperature difference correction factor.

The comparison between the numerical simulation results and the results calculated by the empirical correlation as shown in fig. 4. It is obvious that the results obtained by numerical simulations are consistent with those obtained by empirical correlation. The average error of Nusselt number and f is about 8.4% and 9.2%, respectively. The calculation error or uncertainty caused by the use of the experimental correlation is often more than ±20%, or even higher [19]. So, the numerical method is considered reliable.

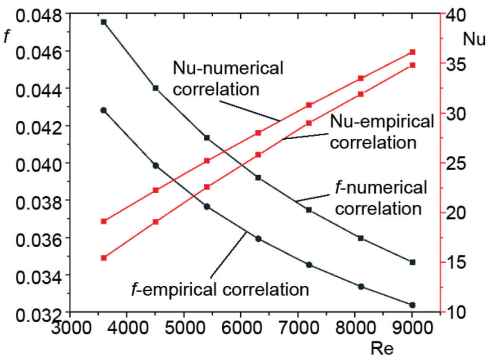

Figure 4. Comparision of numerical simulation and empirical correlation

Results and discussion

Flow field structure

This part mainly discusses the impacts of NVG on the flow field structure in the rectangular channel. Figure 5 shows the velocity streamlines near the NVG at Re = 9004. A pair of vortices with the rotation axis parallel to the mainstream direction is generated from the side walls of the NVG. The boundary-layer will be captured by the vortices. The

continuous separation of the shear layer on the side walls leads to more gas being sucked into the vortex structure, which will reduce the vortex intensity. Therefore, the vortices are captured by increasing the height of the NVG's sidewalls. These vortices sweep towards or away from the bottom surface and move downstream, destroying the boundary-layer near the wall, strengthening the turbulence, and finally enhancing the heat transfer performance of the rectangle channel.

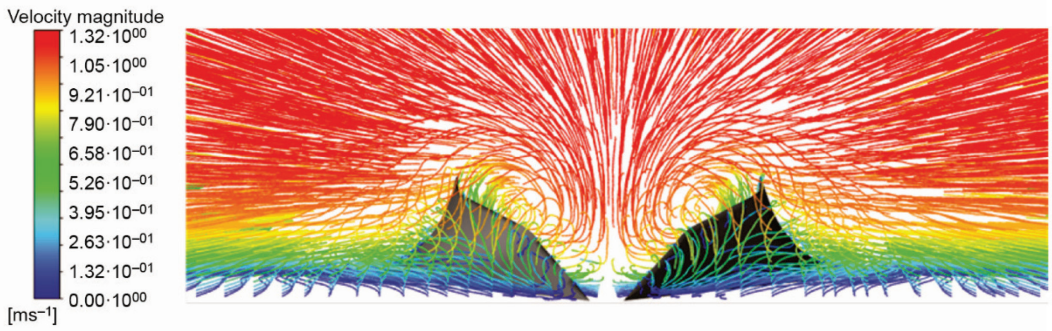

Figure 5. Velocity streamlines near the NVG

Furthermore, the distribution of *X*-vorticity and *Y*-vorticity on the bottom surface along the *y*-axis at three different positions in the freestream direction is shown in fig. 6. As shown in fig. 6(a), a pair of symmetrical vortices of equal size and opposite directions is generated in the flow field, which is consistent with the velocity streamlines diagram in fig. 6. The vortices are especially significant at $x = 0.35$ m, while it is very small before the NVG. At the back position far away from the NVG, the intensity of the vortices decrease gradually. As shown in fig. 6(b), in front of the NVG, the intensity of the transverse vortex is strong. At the back position of the NVG, the *Y*-vorticity has a step change. The *Y*-vorticity is small near the inner wall of the NVG and large near the center. Comparing fig. 6(a) with fig. 6(b), the intensity of the *Y*-vorticity is significantly greater than that of the *X*-vorticity. The vortices induced by the NVG will affect the distribution of the local Nu in the rectangular channel.

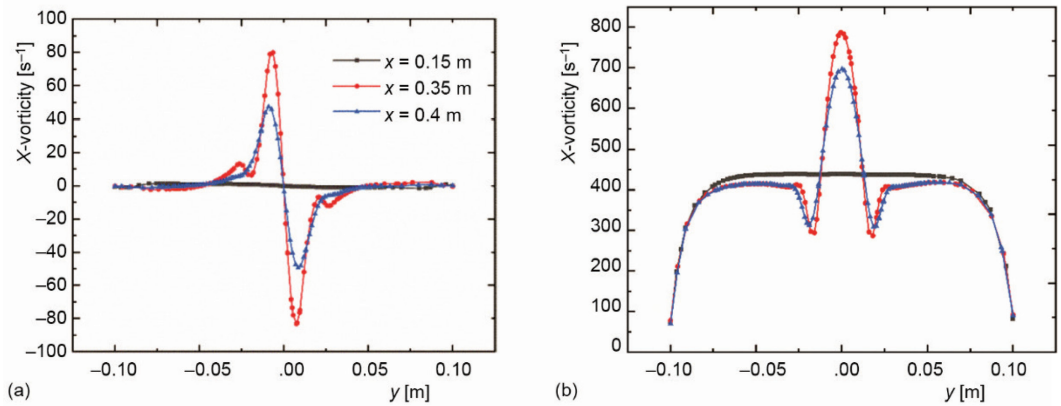

Figure 6. Distribution of vorticity along the *y*-axis; (a) *X*-vorticity and (b) *Y*-vorticity

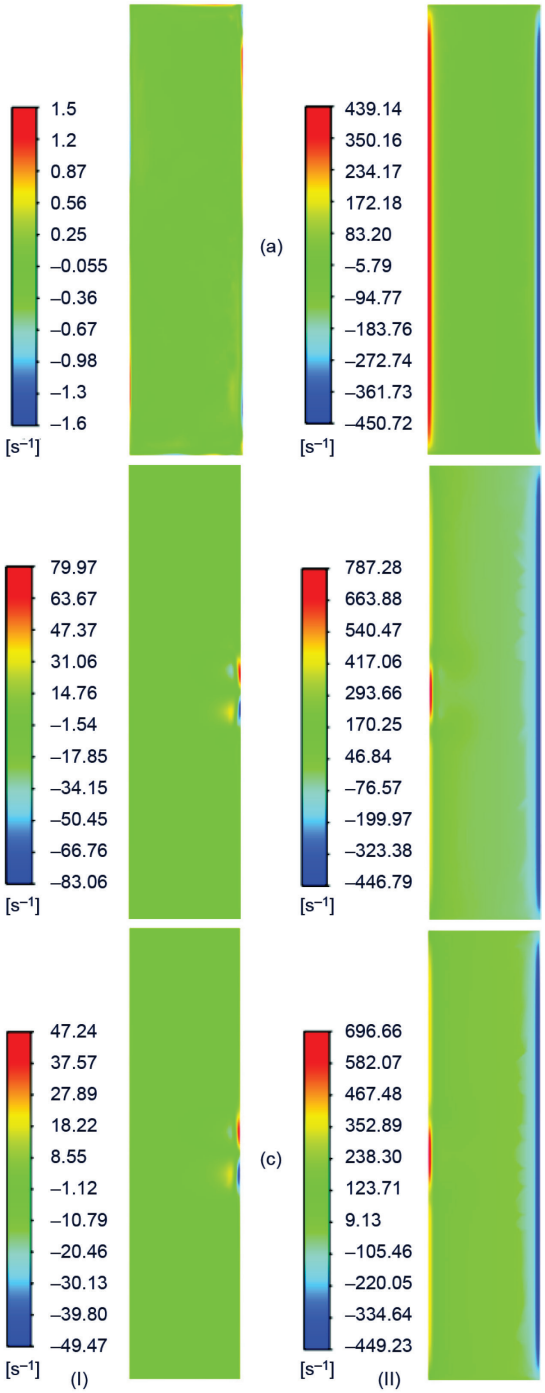

Figure 7. Vorticity distribution contours on different planes: (I) *X*-vorticity and (II) *Y*-vorticity; (a) x = 0.15 m, (b) x = 0.35 m, and (c) x = 0.4 m

Figure 7 shows the distribution contours of *X*-vorticity and *Y*-vorticity at three different planes. The distribution pattern is consistent with fig. 7.

Influence of geometric parameters on the performance

Effects of W

Figure 8 shows the variation of the proportion of average Nusselt number in the presence and absence of the NVG and local Nusselt number at x = 0.4 m along the y-direction at Re = 9004 with four different W. As shown in fig. 8(a), the Nu/Nu_0 shows a consistent trend for NVG with different widths, decreasing continuously as the Reynolds number increase. At low Reynolds number, the effect of NVG is larger than that at high Reynolds number. On the other hand, the ratio of Nu/Nu_0 increases regularly with the increase of W. It shows that the increase of W can enhance the heat transfer of the rectangular channel. This can be explaned by fig. 8(b). It is observed that the change of the local Nusselt number along the y-direction is similar to the distribution of the *Y*-vorticity. At the position of y = 0 m, the vortex intensity is strong, so the average Nusselt number is also large. With the increase of W, it becomes more and more obvious. In addition, the vortices develop in a relatively wide range towards the downstream region. Thus, the increase of W leads to a gradual increase in the average Nusselt number of the whole channel.

It is worth noting that, besides the peak, two troughs also appear near the side walls of the NVG. With the increase of W, the amplitude of the trough increases, and the heat transfer here gradually deteriorates. The generation of flow stagnation zones near the side walls is the primary reason for this phenomenon. As a result, the velocity is small and the turbulence intensity is weak here.

Figure 9 shows the variation of $\Delta p/\Delta p_0$ and η/η_0 in the presence and absence of the NVG with four different W. It can be seen from fig. 9(a) that with the increase of the Reynolds number, $\Delta p/\Delta p_0$ increases first and then decreases. At high Reynolds number, the velocity in the rectangular channel is correspondingly larger, so the pressure loss is also larger. The higher the Reynolds number, the smaller the additional pressure loss resulting from the NVG. With the increase of NVG's width, the pressure loss increases gradually. The NVG with a width of 10 mm obtains the smallest pressure loss, while the one with a width of 30 mm obtains the largest pressure loss. As shown in fig. 9(b), as the W decreases, the η increases, indicating that not only the heat transfer is enhanced, but also there is only a slight increase in pressure loss. Additionally, the heat transfer is not only dependent on W but also negatively related to Reynolds number. The largest η value of 1.042 is obtained by Re = 3602 and W = 10 mm in this case.

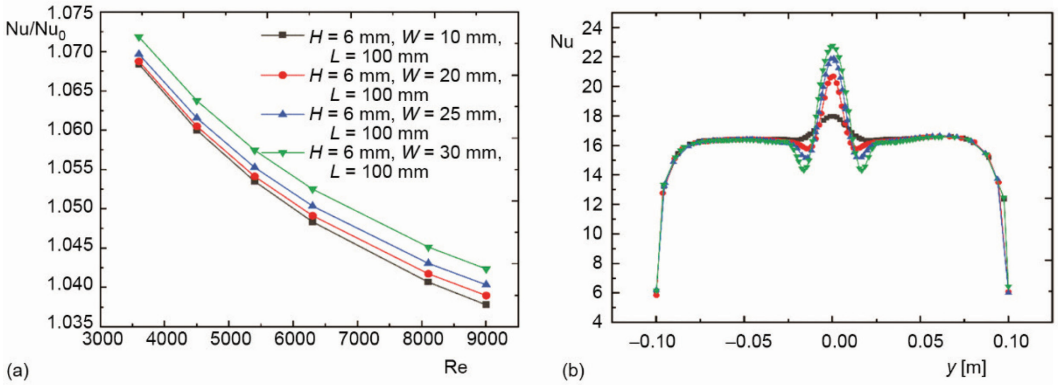

Figure 8. Effect of different W; (a) Nu/Nu_0 and (b) local Nusselt number along the y-axis at Re = 9004

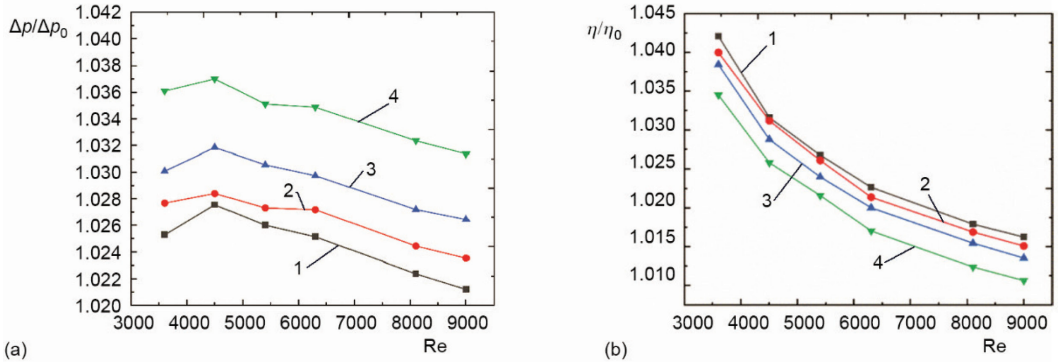

Figure 9. Effect of different W; (a) $\Delta p/\Delta p_0$ and (b) η/η_0: *1 – H = 6 mm, W = 10 mm, L = 100 mm, 2 – H = 6 mm, W = 20 mm, L = 100 mm, 3 – H = 6 mm, W = 25 mm, L = 100 mm, and 4 – H = 6 mm, W = 30 mm, L = 100 mm*

Effects of H

Figure 10 shows the variation of the proportion of average Nusselt number in the presence and absence of the NVG with four different H. It can be found that Nu/Nu_0 decreases as the Reynolds number increases. The maximum reduction is 2.8% in the Reynolds number range studied. With the increase of H, the average Nusselt number increases, which indicates that the increase of H can enhance the heat transfer in the rectangular channel. This can be explained by fig. 11.

Figure 11 shows the proportion of the local Nusselt number along the y-axis at three positions at Re = 9004. The three positions are x = 0.15 m (before the NVG), x = 0.35 m and x = 0.4 m (after the NVG). It can be seen from fig. 11(a), that before the NVG, the local Nusselt number is unchanged, and the NVG have little impact on the heat transfer at this position. As shown in figs. 11(b) and 11(c), after the NVG, the local Nusselt number is significantly enhanced, but its magnitude decreases as the distance increases. In addition, the local Nusselt number is the largest at the center of the channel. The reason is that the vortex intensity at the center of the channel is the largest. This is most obvious in the case of H = 10 mm. Compared with fig. 6, the local Nusselt number is larger at the position with larger vortices. The angle between the velocity vector near the wall and the temperature gradient is very small, so the local heat transfer at these positions is strong [20]. This can also be illustrated by fig. 12. Figure 12 shows the distribution of velocity on the Z = 0.002 m plane at different H. The local Nusselt number distribution in fig. 11 is consistent with the velocity distribution in fig. 12.

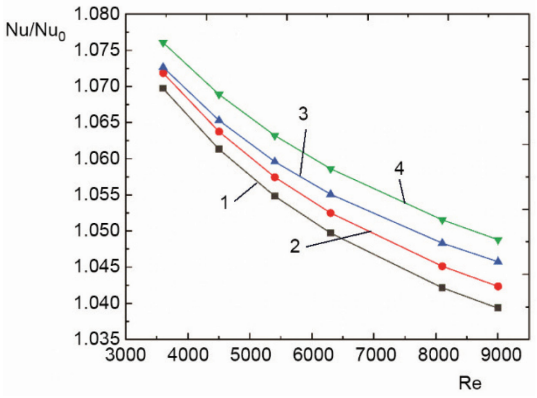

Figure 10. Effect of different H on Nu/Nu$_0$: *1 – H = 4 mm, W = 30 mm, L = 100 mm, 2 – H = 6 mm, W = 30 mm, L = 100 mm, 3 – H = 8 mm, W = 30 mm, L = 100 mm, and 4 – H = 10 mm, W = 30 mm, L = 100 mm*

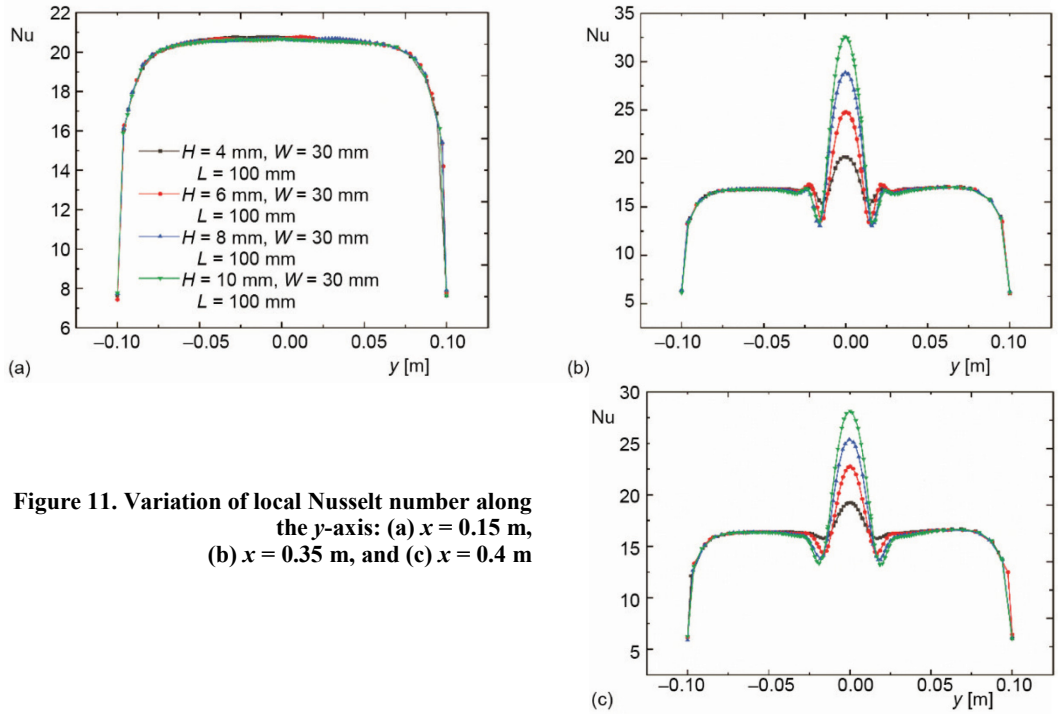

Figure 11. Variation of local Nusselt number along the y-axis: (a) x = 0.15 m, (b) x = 0.35 m, and (c) x = 0.4 m

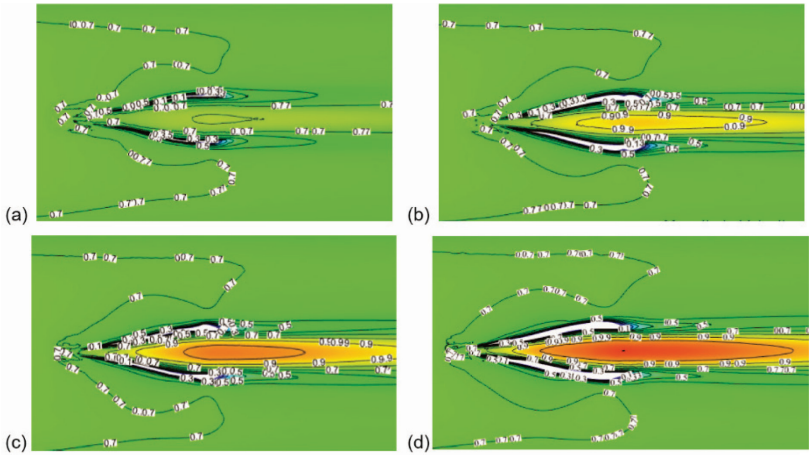

Figure 12. Velocity distribution on the Z = 0.002 m plane at different H; (a) H = 4 mm, (b) H = 6 mm, (c) H = 8 mm, and (d) H = 10 mm

Figure 13 shows the variation of $\Delta p/\Delta p_0$ and η/η_0 in the presence and absence of the NVG with four different H. As can be seen from fig. 13(a), the pressure loss increases gradually with the increase of H. The largest and smallest pressure loss is obtained by H = 10 mm and H = 4 mm, respectively. As can be seen from fig. 13(b), the smaller the H, the larger the η. The largest η value of 1.04 is obtained by Re = 3602 and H = 4 mm in this case.

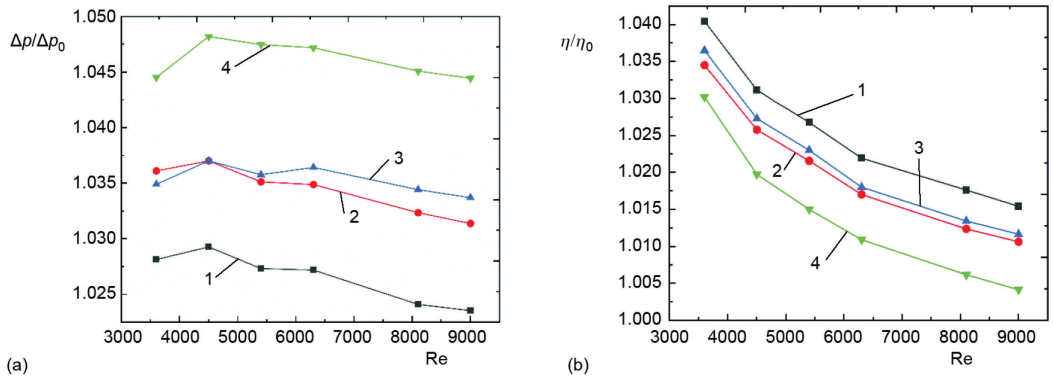

Figure 13. Impact of different H; (a) $\Delta p/\Delta p_0$ and (b) η/η_0: *1 – H = 4 mm, W = 30 mm, L = 100 mm, 2 – H = 6 mm, W = 30 mm, L = 100 mm, 3 – H = 8 mm, W = 30 mm, L = 100 mm, and 4 – H = 10 mm, W = 30 mm, L = 100 mm*

Conclusions

Characteristics of the flow and heat transfer of the NVG in the rectangular channel were studied numerically. The distribution of the vortices is investigated. The impacts of the W (10 mm, 20 mm, 25 mm, and 30 mm) and H (4 mm, 6 mm, 8 mm, and 10 mm) of the NVG on the pressure loss, heat transfer, and comprehensive performance were investigated. The

influence of Reynolds number (range from 3602 to 9004) is also studied. The results are concluded as follows:

Improved heat transfer can be obtained due to the use of NVG, which is more pronounced at low Reynolds number.

– The local average Nusselt number can be improved significantly due to the vortices induced by the NVG. The variation of the local Nusselt number is similar to that of the *Y*-vorticity.
– With the increase of *W* and *H*, the average Nusselt number and the pressure loss increase gradually. The average Nusselt number increases by about 7.3%, and the pressure loss increases by about 3.6% by $H = 6$ mm, $W = 30$ mm, and $L = 100$ mm at Re = 3602. The average Nusselt number increases by about 7.6%, and the pressure loss increases by about 4.5% by $H = 10$ mm, $W = 30$ mm, and $L = 100$ mm at Re = 3602.
– The variation of comprehensive performance is the opposite. High comprehensive performance can be obtained by $W = 10$ mm and $H = 4$ mm at Re = 3602, respectively.

Nomenclature

A – heat transfer area, [m^2]
C_p – specific heat
d – characteristic length, [m]
f – Darcy drag factor
h – convective heat transfer factor, (= $Q/A/\Delta T$) [$Wm^{-2}K^{-1}$]
H – height of NVG, [mm]
L – length of NVG, [mm]
p – pressure, [Pa]
Pr – Prandtl number(= $C_p\mu/\lambda$)
Q – heat transfer rate, [W]
Re – Reynolds number(= $\rho ud/\mu$)
T – temperature, [K]
T_{wall} – temperature of the wall, [K]
u – velocity, [m/s]
W – width of NVG, [mm]
Δp – total pressure loss, [Pa]

Greek symbols

η – comprehensive criterion
λ – thermal conductivity, [$Wm^{-1}K^{-1}$]
μ – dynamic viscosity, [Pas]
μ_t – turbulent viscosity, [Pas]
ρ – density, [kgm^{-3}]

Subscripts

0 – smooth rectangular channel
test_in – the inlet of test section
test_out – the outlet of test section

Acronyms

NVG – NACA vortex generator
VG – vortex generator
TWP – trapezoidal winglet pair
CTWP – curved trapezoidal winglet pair
NACA – National Advisory Committee for Aeronautics
RMS – response surface methodology
DOM – direct optimization method

References

[1] Tian, L., *et al*., Heat Transfer Performance Comparison of Wavy Finned Tube Heat Exchanger with Delta Winglets Under Different Arrays, *Journal of Power Engineering*, *29* (2009), 1, pp. 78-83
[2] Ni, Y., Development of the Vortex Generator and Study on the Effect of Vortex Generator on Boundary-layer, *Acta Aerodynamica Sinica*, *13* (1995), 1, pp. 110-116
[3] Su, S., *et al*., Wang, Flow and Heat Transfer Characteristics of Finned Tube Heat Exchanger with Arc Delta Winglets, *Journal of Chinese Society of Power Engineering*, *33* (2013), 3, pp. 194-198
[4] Silva, F., *et al*., Longitudinal Vortex Generator Applied to Heat Transfer Enhancement of a Flat Plate Solar Water Heater, *Applied Thermal Engineering*, *158* (2019), 113790
[5] Song, K., *et al*., Heat Transfer Characteristics of Concave and Convex Curved Vortex Generators in the Channel of Plate Heat Exchanger Under Laminar Flow, *International Journal of Thermal Sciences*, *137* (2019), Mar., pp. 215-228
[6] Hu, D., *et al*., Performance Optimization of a Wavy Finned-Tube Heat Exchanger with Staggered Curved Vortex Generators, *International Journal of Thermal Sciences*, *183* (2023), 107830
[7] Khanjian, A., *et al*., Effect of Rectangular Winglet Pair Roll Angle on the Heat Transfer Enhancement in Laminar Channel Flow, *International Journal of Thermal Sciences*, *114* (2017), Apr., pp. 1-14

[8] Moreno, R., *et al*., Numerical Optimization of a Heat Exchanger with Slit Fins and Vortex Generators Using Genetic Algorithms, *International Journal of Refrigeration*, *119* (2020), Nov., pp. 247-256
[9] Salviano, L., *et al*., Optimization of Winglet-Type Vortex Generator Positions and Angles in Plate-Fin Compact Heat Exchanger: Response Surface Methodology and Direct Optimization, *International Journal of Heat and Mass Transfer*, *82* (2015), Mar., pp. 373-387
[10] Esmaeilzadeh, A., *et al*., Comparison of Simple and Curved Trapezoidal Longitudinal Vortex Generators for Optimum Flow Characteristics and Heat Transfer Augmentation in a Heat Exchanger, *Applied Thermal Engineering*, *125* (2017), Oct., pp. 1414-1425
[11] Sun, Z., *et al*., Experimental and Numerical Studies of Intensified Turbulent Heat Transfer in Round Pipes with Curved Wing Vortex Generators, *International Journal of Heat and Mass Transfer*, *180* (2021), 121823
[12] Pei, H., *et al*., Structural Parameters Optimization of Submerged Inlet Using Least Squares Support Vector Machines and Improved Genetic Algorithm-Particle Swarm Optimization Approach, *Engineering Applications of Computational Fluid Mechanics*, *15* (2021), 1, pp. 503-511
[13] Cui, Y., *et al*., Parametric Modeling of NACA Air Inlet Based on Catia, *Aeronautical Computing Technique*, *50* (2020), 2, pp. 68-71
[14] Wu, X., *et al*., Numerical Simulation of Heat Transfer and Fluid-flow Characteristics of Composite Fin, *International Journal of Heat and Mass Transfer*, *75* (2014), Aug., pp. 414-424
[15] Pei, H., *et al*., Flow and Heat Transfer Characteristics of a Novel Airfoil-Based Tube with Dimples, *Bulletin of the Polish Academy of Sciences:Technical Sciences*, *70* (2022), 4, 141984
[16] Xie, S., *et al*., A Numerical Study on Heat Transfer Enhancement and Flow Structure in Enhanced Tube with Cross Ellipsoidal Dimples, *International Journal of Heat and Mass Transfer*, *125* (2018), Oct., pp. 434-444
[17] Oh, Y., Kim, K., Effects of Position and Geometry of Curved Vortex Generators on Fin-Tube Heat-Exchanger Performance Characteristics, *Applied Thermal Engineering*, *189* (2021), 116736
[18] Yang, S., *Heat Transfer*, Beijing: Higher Education Press, Beijing, China, 2006
[19] Li, M., *et al*., Geometric Optimization for the Thermal-Hydraulic Performance of Dimpled Enhanced Tubes for Single Phase Flow, *Applied Thermal Engineering*, *103* (2016), June, pp. 639-650
[20] Zhao, Z., *Heat Transfer*, Beijing: Higher Education Press, Beijing, China, 2002
[21] Guo, Z., *et al*., A Novel Concept for Convective Heat Transfer Enhancement, *International Journal of Heat and Mass Transfer*, *41* (1998), 14, pp. 2221-2225

Paper submitted: December 31, 2022
Paper revised: March 1, 2023
Paper accepted: March 6, 2022